

Cite this: DOI: 00.0000/xxxxxxxxxx

Materials Discovery with Extreme Properties via Reinforcement Learning-Guided Combinatorial Chemistry[†]

Hyunseung Kim,^{a,‡} Haeyeon Choi,^{b,c,‡} Dongju Kang,^{a,‡} Won Bo Lee,^{*a} and Jonggeol Na^{*b,c}Received Date
Accepted Date

DOI: 00.0000/xxxxxxxxxx

The goal of most materials discovery is to discover materials that are superior to those currently known. Fundamentally, this is close to extrapolation, which is a weak point for most machine learning models that learn the probability distribution of data. Herein, we develop reinforcement learning-guided combinatorial chemistry, which is a rule-based molecular designer driven by trained policy for selecting subsequent molecular fragments to get a target molecule. Since our model has the potential to generate all possible molecular structures that can be obtained from combinations of molecular fragments, unknown molecules with superior properties can be discovered. We theoretically and empirically demonstrate that our model is more suitable for discovering better compounds than probability distribution-learning models. In an experiment aimed at discovering molecules that hit seven extreme target properties, our model discovered 1,315 of all target-hitting molecules and 7,629 of five target-hitting molecules out of 100,000 trials, whereas the probability distribution-learning models failed. Moreover, it has been confirmed that every molecule generated under the binding rules of molecular fragments is 100% chemically valid. To illustrate the performance in actual problems, we also demonstrate that our models work well on two practical applications: discovering protein docking molecules and HIV inhibitors.

1 Introduction

The task of discovering materials that are superior to those currently known is a challenging problem in various fields of materials science, including pharmaceutical substances^{1–4}, electrical and electronic materials^{5–11}, energy materials^{11–14}, metals and ceramics¹⁰, nanomaterials¹⁵, and polymeric materials^{16,17}. Some of these studies aim to discover materials with two or more target properties that contradict each other, meaning it is difficult for them to coexist¹⁸. For example, super engineering plastics used in automobiles should be lighter than metals yet have similar mechanical strength^{16,17}. Similarly, transparent conductors used in display panels should be both optically transparent (requiring a large bandgap) and electrically conductive (requiring high carrier concentration, which generally has a low bandgap)^{5,18}. In some cases, the aim is to discover materials that have properties with either extremely high or low values. For example, the development of a better organic light-emitting diode (OLED) re-

quires chemists to discover novel materials with higher efficiency and stability^{6–8}. Here, the problem is that there are no (or few) known samples that have such properties compared to common substances. This makes it difficult for chemists to gain insights or knowledge from the known materials, that could help to infer the molecular structures of the desired materials. Unfortunately, this situation also holds for most machine learning models that learn the data. Therefore, it is necessary to develop a model that can discover materials, even in regions with little or no known data. In this paper, we refer to this problem as *materials extrapolation*.

In recent years, it has been reported that machine learning techniques can solve many challenging problems in a wide range of fields, including materials discovery. In particular, models for goal-directed inverse molecular design are attractive because they can directly infer the molecular structures that meet a set of given target conditions such as scaffolds^{2,21}, physical properties^{15,22–24}, and biological activities^{2,4,24}. Some of these studies have proposed models based on neural machine translation (NMT) such as seq2seq^{24,25} and Transformer²⁶, which translate input target conditions to corresponding molecular structures. Models based on conditional generative models have also been proposed, such as conditional generative adversarial networks (cGANs)²⁷ and conditional variational autoencoders (cVAEs)²⁸. These models directly generate molecular structures to meet a set of given target conditions^{15,21–23}. In contrast, there are also ways to obtain the desired materials from unconditional gener-

^a School of Chemical and Biological Engineering, Seoul National University, Republic of Korea; E-mail: wblee@snu.ac.kr

^b Department of Chemical Engineering and Materials Science, Ewha Womans University, Republic of Korea; E-mail: jgna@ewha.ac.kr

^c Graduate Program in System Health Science and Engineering, Ewha Womans University, Republic of Korea

[†] Electronic Supplementary Information (ESI) available: [details of any supplementary information available should be included here]. See DOI: 00.0000/00000000.

[‡] These authors contributed equally to this work.

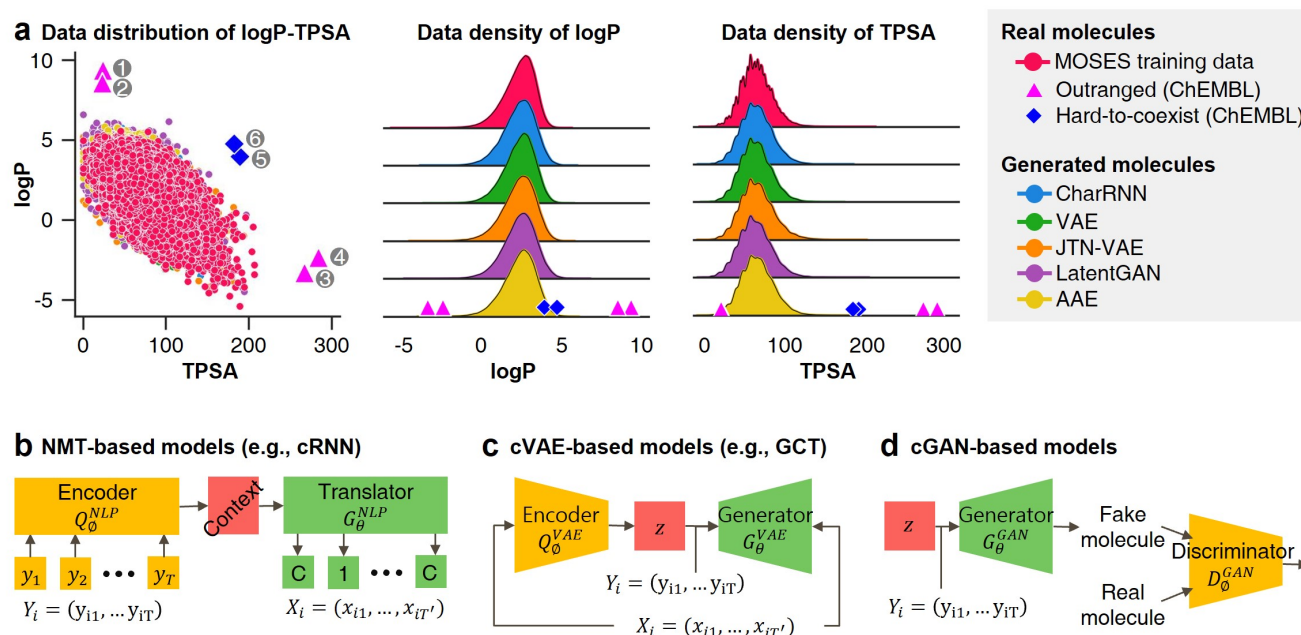


Fig. 1 Probability distribution-learning models for molecular generation. (a) Data distribution of logP-TPSA. The pink dots denote the molecules in MOSES¹⁹ training data. The other colored dots denote the molecules generated by MOSES baseline models which were trained with the MOSES training data. Since the MOSES baseline models are probability distribution-learning models such as NMT, GAN, VAE, and AAE, the distribution of generated molecules approximates the distribution of their training data. The magenta triangles and blue diamonds indicate real molecules in ChEMBL²⁰ database, which have extrapolated properties from MOSES training data distribution. ① CHEMBL3216345; ② CHEMBL3230084; ③ CHEMBL3358630; ④ CHEMBL300801; ⑤ CHEMBL501130; ⑥ CHEMBL52004. (b-d) Types of inverse molecular designer. X_i , Y_i , and z denote i -th molecular structure, properties of the i -th molecule, and latent code, respectively.

ative models, such as generative adversarial networks (GANs)²⁹ and variational autoencoders (VAEs)³⁰. These approaches use additional methods to find appropriate latent code, which is required to generate the target-hitting substances. Navigating policies of latent space trained by reinforcement learning (RL)^{31,32} and optimization techniques^{33–35} belong here.

Unfortunately, all of the previously mentioned models (NMT, GAN, and VAE-based) are difficult to use in materials extrapolation for discovering novel materials with properties that are out of training data distribution. To generate realistic molecules with these models, the models should be trained to generate molecular data that approximate the probability distribution of the real-world chemical system. However, since it is impossible to know the true probability of the real-world chemical system, the models are trained to generate data that approximate the empirical probability of the training data. Regrettably, the empirical data at our disposal may exhibit biases due to various factors, consequently leading to models trained on such biased data failing to generate some molecules that even exist in the real world (Fig. 1a). Hence, the probability distribution-learning models are not suitable for generating molecules in regions with little or no known data (such as materials extrapolation). Furthermore, there are several ongoing discussions about whether probability distribution-learning models are suitable for extrapolation problems^{9,10,19,36}. In the same vein, we believe that employing an approach that either avoids using data or minimizes data usage, such as RL and genetic algorithm (GA), is appropriate for materials extrapolation. Since GA is a method for deriving a set of optimal solutions

rather than a problem-solving policy, it cannot guarantee the diversity of the derived solution set. On the contrary, RL involves learning action policies to obtain solutions based on the given current state. This advantage enables RL to infer a wider variety of solutions. Therefore, we intend to utilize RL in our approach. Despite several recent studies utilizing RL in molecular design^{2,4,37}, the majority of them do not prioritize presenting RL as a means to address the limitations of probability distribution-learning models for discovering substances beyond their trained domains.

Combinatorial chemistry³⁸ was invented in the 1980s and can generate molecules with properties out of known data. These types of methods use a set of molecular fragments and rules for fragment combination. Breaking of retrosynthetically interesting chemical substructures (BRICS)³⁹ is an example of combinatorial chemistry. This technique involves combining randomly selected BRICS fragments with their template-based fragment combination rules, which is similar to assembling Lego blocks. Therefore, combinatorial chemistry can create all chemically possible molecular structures that can be obtained from the combination of molecular fragments. According to our estimation, approximately 4×10^{16} types of small molecules (≤ 500 Da) can be combined with 2,207 BRICS fragments. Considering that the total number of small molecules was roughly estimated to be 10^{60} in ref.⁴⁰, this means that it can cover a fairly wide area. However, there is the limitation that the combinatorial chemistry-based molecular generator does not know which molecular fragments to be selected and combined to complete the desired molecule. In other words, it has no policy to guide the selection of molecular fragments to

obtain the target molecule. Hence, it proceeds with countless attempts to combine randomly selected fragments and selects the best compound from the generated molecular candidates, which can result in a combinatorial explosion⁴¹. If we assume that it takes 1 *ms* to assemble one molecule, it would take 1.27×10^6 years to enumerate all possible small organic molecules using 2,207 molecular fragments; 4×10^{16} molecules $\times 1$ *ms* = 1.27×10^6 years.

Herein, we introduce RL to provide combinatorial chemistry with a molecular fragment selection policy that guides the generating molecule toward the target. With a randomly selected initial fragment, the RL-guided policy iteratively selects the subsequent fragment to be combined. In the training phase, the policy is learned by giving a higher reward if the properties of the generated molecule are closer to the target. Therefore, the learned policy enables an efficient search of chemical space and helps to escape from the combinatorial explosion problem by providing direction to the target. Moreover, the proposed model—*RL-guided combinatorial chemistry (RL-CC)*—has the potential to enable materials extrapolation, which is impossible for probability distribution-learning models. To demonstrate the potential empirically, we apply RL-CC and two probability distribution-learning models to a toy problem of molecules discovery that hits multiple extreme target properties simultaneously. The results indicate that our model can discover extreme target molecules that probability distribution-learning models cannot reveal. Furthermore, we theoretically demonstrate why the probability distribution-learning models are not suitable for problems involving materials extrapolation. To illustrate the performance in actual problems, we conduct two practical experiments. The first is to discover protein docking molecules to a 5-hydroxytryptamine receptor 1B (5-HT_{1B} receptor) with high binding affinity. The second is the discovery of human immunodeficiency virus (HIV) inhibitors with high potency. These two experiments demonstrate that the proposed approach can discover compounds with extreme properties, which shows the potential to be extended as materials extrapolation when it utilizes a set of domain-specific molecular fragments and their combination rules.

2 Results and Discussion

2.1 Theoretical review of probability distribution-learning models

Inverse molecular design models based on NMT, VAE, and GAN learn the empirical probability distribution of training data P_{data} . Let $X, Y = (X_1, Y_1), \dots, (X_N, Y_N)$ denote N -sampled training data. Here, $X_i = (x_{i,1}, \dots, x_{i,T'})$ denotes sequence data of the i -th molecular structure, and $Y_i = (y_{i,1}, \dots, y_{i,T})$ denotes a set of properties of the i -th molecule. The NMT-based models are trained to translate the input $Y_i = (y_{i,1}, \dots, y_{i,T})$ into a paired output sequence $X_i = (x_{i,1}, \dots, x_{i,T'})$. Here, $x_{i,t}$ is a one-hot encoded vector of the t -th token constituting a molecule X_i . The θ -parameterized translator G_{θ}^{NLP} should be trained to select a token $x_{i,t}$ iteratively over $t = 1, \dots, T'$, by maximizing the likelihood $\prod_{i=1}^N \prod_{t=1}^{T'} G_{\theta}^{NLP}(x_{i,t} | Y_i, x_{i,1:t-1})$ empirically. The actual training process is conducted by minimizing its negative log-likelihood

$-\sum_{i=1}^N \sum_{t=1}^{T'} \log G_{\theta}^{NLP}(x_{i,t} | Y_i, x_{i,1:t-1})$, which is equivalent to minimizing cross-entropy $H(\cdot, \cdot)$ of hypothesis \hat{X}_{θ} from training data X :

$$\begin{aligned} H(X, \hat{X}_{\theta}) &= -\sum_{i=1}^N \sum_{t=1}^{T'} P(X) \log P(\hat{X}_{\theta}) \\ &= H(X) + D_{KL}(P(X) \| P(\hat{X}_{\theta})) \end{aligned} \quad (1)$$

where $H(X) = -\sum_{i=1}^N \sum_{t=1}^{T'} P(X) \log P(X)$ denotes the entropy⁴² of training data X , and $D_{KL}(P(X) \| P(\hat{X}_{\theta}))$ is the Kullback–Leibler (KL) divergence⁴³ of hypothesis probability $P(\hat{X}_{\theta})$ from P_{data} . Since $H(X)$ is not a function of trainable parameter θ , minimizing the cross-entropy $H(X, \hat{X}_{\theta})$ is equivalent to minimizing the KL divergence term in Equation (1). Thus, the optimal G_{θ}^{NLP} is obtained by approximating $P(\hat{X}_{\theta})$ —which is the probability distribution of data generated by G_{θ}^{NLP} —to P_{data} . It means that G_{θ}^{NLP} learns the empirical probability distribution of training data P_{data} , not the true probability distribution of the system P .

Second, VAE-based models are types of generative self-learning models that learn the empirical probability distribution of training data P_{data} . The models are trained to encode training data $X = X_1, \dots, X_N$ in the latent space with encoder Q_{ϕ}^{VAE} and reconstruct it with decoder G_{θ}^{VAE} . The difference from autoencoders is that the latent variables z are constrained to follow a prior distribution such as a normal distribution. The VAEs are trained using the following objective function³⁰:

$$\arg \min_{\phi, \theta} \sum_{i=1}^N -\mathbb{E}_{Q_{\phi}^{VAE}(z|X_i)} \left[\log G_{\theta}^{VAE}(X_i | z) \right] + D_{KL} \left(Q_{\phi}^{VAE}(z | X_i) \| P(z) \right) \quad (2)$$

When looking at the VAEs from the perspective of a generative model, the KL divergence term simply acts like a regularizer in the training process. The expectation term measures the reconstruction error of G_{θ}^{VAE} and it is approximated by using the following L -number of Monte-Carlo sampling:

$$-\mathbb{E}_{Q_{\phi}^{VAE}(z|X_i)} \left[\log G_{\theta}^{VAE}(X_i | z) \right] \approx -\frac{1}{L} \sum_{z_j=1}^L \log \left(G_{\theta}^{VAE}(X_i | z_j) \right) \quad (3)$$

Here, the approximated reconstruction error term is a form of negative log-likelihood over training data X . Hence, it is equivalent to minimizing the cross-entropy $H(\cdot, \cdot)$ of hypothesis $\hat{X}_{\theta,z}$ from training data X :

$$\begin{aligned} H(X, \hat{X}_{\theta,z}) &= -\sum_{i=1}^N \sum_{t=1}^{T'} P(X) \log P(\hat{X}_{\theta,z}) \\ &= H(X) + D_{KL}(P(X) \| P(\hat{X}_{\theta,z})) \end{aligned} \quad (4)$$

As mentioned above, this is also equivalent to minimizing the KL divergence term in Equation (4), since $H(X)$ is not a function of trainable parameter θ . Hence, the optimal G_{θ}^{VAE} is obtained by approximating the probability distribution of hypothesis $P(\hat{X}_{\theta,z})$

to the P_{data} . This means that $G_{\theta}^{VAE}(X|z)$ with $z \sim Q_{\phi}^{VAE}(z|X)$ approximates P_{data} .

Third, GAN is also a model to obtain a generator G_{θ}^{GAN} that approximates P_{data} . Here, G_{θ}^{GAN} learns the P_{data} in the learning process to generate data that sufficiently resembles training data X to deceive the discriminator D_{ϕ}^{GAN} . Note that it has been proved that the global minimum of the virtual training criterion of the generator is achieved if (and only if) $P_{data} = G_{\theta}^{GAN}(z)$ ²⁹. This means that the optimal G_{θ}^{GAN} is obtained by approximating the hypothesis probability $P(\hat{X}_z)$ to the probability of training data P_{data} .

Therefore, it can be concluded that models based on NMT, VAE, and GAN used for inverse molecular design are models to derive an approximator of P_{data} . Unfortunately, since P_{data} derived from the observed empirical data is not equal to the true probability P of chemical system, it cannot guarantee that the probability-distribution learning models will work well for problems involving materials extrapolation.

2.2 RL-guided combinatorial chemistry with BRICS

The RL-CC illustrated in Fig. 2 is applicable to various tasks of materials discovery, by designing a target molecule with the selected molecular fragments. A trained RL-guided policy iteratively selects the subsequent fragment to be combined. Here, the RL-guided policy serves as a guide to generate a target-hitting molecule. This approach has three main phases: configuration settings (Fig. 2b–d), training (Fig. 2a), and inference (Fig. 3).

In the configuration settings phase, all settings necessary for reinforcement learning are customized. Accordingly, the task for materials discovery must be specified. There are two types of tasks for this (Fig. 2c): the discovery of molecules to hit specific values of the multiple target properties (Task type A), and the discovery of molecules to maximize a specific property (Task type B). Depending on the type of given task, the user designs the reward function r , target error function ϵ , termination conditions c_{term} , and target conditions c_{trg} . The reward function r is designed to give a higher reward the better a given task is performed. For Task type A, the target error function ϵ and reward function r are designed as sum errors for the multiple target properties and the reciprocal of the target error function ϵ , respectively. In the case of Task type B, the property itself is used as the reward function r ; hence, maximizing r is equivalent to maximizing the property. For the minimization case of Task type B, the negative property is used as the reward function r . We can also consider the constraints p , which are reflected in the reward function r by giving penalties if one of the constraints p is not satisfied. Here, the minimum molecular weight (MW_{min}) and the minimum number of fragments (n_{min}) that make up a molecule can be used as constraints p . These enable the model to generate various molecules by preventing premature termination, which would cause the generation of molecules that were too small and uniform.

The termination conditions (c_{term}) and target conditions (c_{trg}) pertain to deciding when to terminate the process of selecting and combining additional molecular fragments, which determines the characters of the final output molecule. Hence, the termination

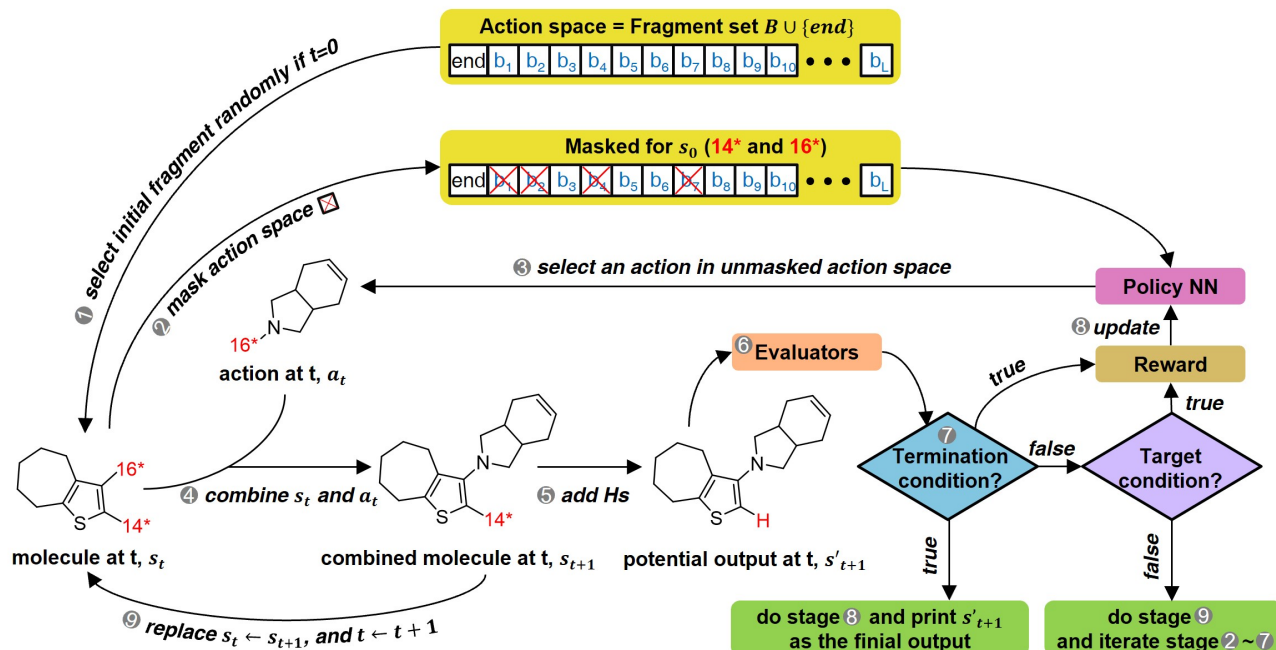
conditions c_{term} and target conditions c_{trg} are designed considering the given task. The molecular generation process is terminated early if one of the termination conditions c_{term} is satisfied. Accordingly, maximum molecular weight (MW_{max}) and maximum number of fragments (n_{max}) are used to design the termination conditions c_{term} . It should be noted that the process is also terminated if there are no more sites for binding fragments to the combined molecule at step t (s_{t+1}) or if the policy selects *end*-action at step t . These are included in the termination conditions c_{term} . The target conditions c_{trg} are the target bounds to hit, which are applied only to Task type A.

To evaluate the previously mentioned functions and conditions, the evaluators (stage 6 in Fig. 2a) for the interesting properties are utilized selectively to calculate the properties of potential output molecule at step t (s'_{t+1}). In order to calculate the properties of the molecule, the molecule must not have any unfilled binding site. Hence, s'_{t+1} is derived by attaching hydrogen to the unfilled binding sites of the combined molecule at step t (s_{t+1}) if s_{t+1} has any unfilled binding site (stage 5 in Fig. 2a). RDKit⁴⁴ was selectively used to evaluate the calculated octanol-water partition coefficient ($\log P$)⁴⁵, topological polar surface area (TPSA)⁴⁶, quantitative estimates of drug-likeness (QED)⁴⁷, number of hydrogen bond acceptors (HBA), number of hydrogen bond donors (HBD), and molecular weight (MW). A quantitative structure-activity relationship (QSAR) model²⁴ and QVina2⁴⁸, which is a tool for discovering the minimum-energy docking conformation of a tested molecule and calculating its docking score, are also selectively used to evaluate drug activity for dopamine receptor D2 (DRD2) and the binding affinity to the 5-HT_{1B} receptor, respectively.

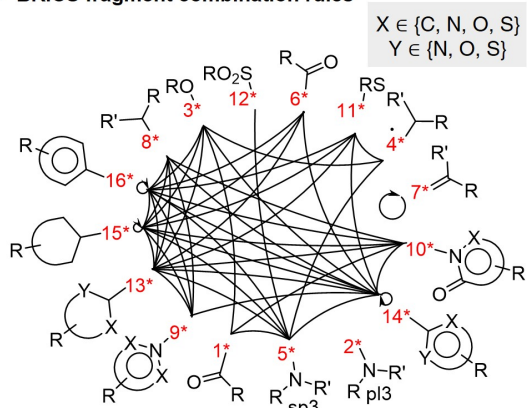
For combinatorial chemistry, fragment set B and its combination rules should be set. Accordingly, a modified version⁴⁴ of the BRICS³⁹ system was adopted (Fig. 2b,d). Since the best performance was achieved for approximately 2k action spaces in the preliminary experiments (ESI† Note 2), approximately 2k fragments were sampled from BRICS 40k for fragment set B . The BRICS fragment combination rules are rules to bind 16 molecular templates, where each template has a unique binding site (red digit in Fig. 2b).

In the training phase, our model was trained using the proximal policy optimization (PPO) algorithm⁴⁹, which is known to perform well in RL problems with discrete actions. This is because it has the advantages of stable training, sample efficiency, scalability, and flexibility. In the preliminary experiments, PPO performed optimally for our problem among several state-of-the-art RL algorithms (ESI† Note 3). An episode iteratively proceeds the process of selecting and combining molecular fragments from steps 0 to T (Fig. 2a). If one of the termination conditions c_{term} or target conditions c_{trg} are satisfied, the episode is prematurely terminated at the step. At step 0, an episode is started with a randomly selected fragment s_0 (stage 1 in Fig. 2a), and the randomness of the initial fragment s_0 creates more diverse output molecules s'_{T+1} . Subsequently, action masking (stage 2 in Fig. 2a) is performed, which masks the actions that are not applicable to s_0 . Thereby, the fragment selection policy is enforced not to select the masked actions. This action masking helps to generate molecules that do not violate the chemical valence rule and en-

a Training process



b BRICS fragment combination rules



c Task type A

Hit target $y_s = \{\log P, \text{TPSA}, \text{QED}, \dots\}$

$$\varepsilon = \sum_{y \in y_s} \left[\frac{y_{\text{target}} - y_{\text{evaluated}}}{\sigma_y} \right]^2$$

$p = \text{penalty if } \{\text{MW} \leq \text{MW}_{\text{min}}, \dots\}$

$c_{\text{term}} = \{\text{MW} \geq \text{MW}_{\text{max}}, a_t = \text{'end'}, \dots\}$

$c_{\text{trg}} = \{\varepsilon \leq \varepsilon_{\text{th}}\}$

$r = 1/\varepsilon$ or p

Task type B

Maximize prop. α

$\varepsilon = \text{None}$

$p = \text{penalty if } \{\text{MW} \leq \text{MW}_{\text{min}}, \dots\}$

$c_{\text{term}} = \{\text{MW} \geq \text{MW}_{\text{max}}, a_t = \text{'end'}, \dots\}$

$c_{\text{trg}} = \text{None; go to 'false'}$

$r = \alpha$ or p

d Fragment set B ~2k

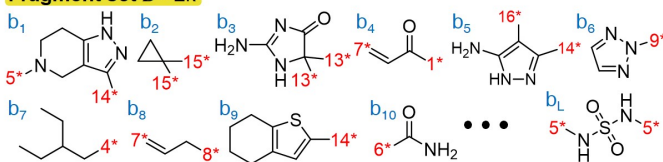


Fig. 2 Overview of RL-guided combinatorial chemistry with BRICS. (a) Training process. (b) Modified BRICS³⁹ fragment combination rules. Here, the RDKit⁴⁴ version 2020.09.1.0 of the modified BRICS rules is adopted. This figure is modified from Degen et al., 2008, *ChemMedChem*, 10(3): 1503-1507³⁹, with permission of Wiley-VCH GmbH. (c) Type of tasks. Task type A is to discover molecules that hit the specific values of given target properties and Task type B is to discover molecules that maximize the given target properties. (d) Fragment set B. Here, $B \cup \{\text{end}\}$ is defined as action space.

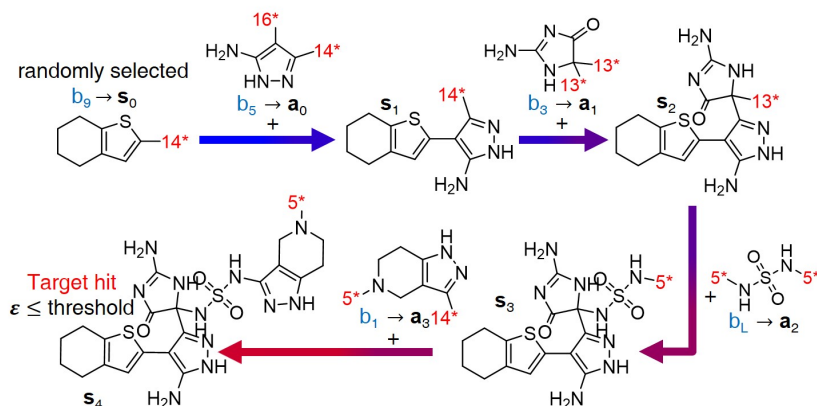
ables efficient learning by reducing the action space. In this way, the fragment selection policy selects an action at step 0 (a_0) from the unmasked actions.

If the selected action at step t (a_t) is the *end*-action, the process is terminated. However, if a_t is a fragment, a_t is combined with s_t to make a combined molecule at step t (s_{t+1}). To evaluate the properties of a molecule, the molecule should not have any unfilled binding sites. Hence, the potential output molecule at step t (s'_{t+1}) is derived by attaching hydrogen to the remaining binding site of s_{t+1} . Then, the interesting properties of s'_{t+1} are evaluated to obtain the target error ε_{t+1} and reward r_{t+1} at step t . Now, to check whether one of the termination conditions c_{term} or target

conditions c_{trg} is satisfied, a_t , ε_{t+1} , and r_{t+1} are considered. If one of the termination conditions c_{term} or target conditions c_{trg} is satisfied, the reward r_{t+1} is used to update the policy. If any of the termination conditions c_{term} and target conditions c_{trg} is not satisfied, the environment outputs the combined molecule s_{t+1} . Then, the model iteratively proceeds to the next step of the process until either one of the termination conditions c_{term} or target conditions c_{trg} is satisfied. This process is repeated for a preset number of iterations to train the model.

After the training is completed, the trained policy is used to generate a target molecule in the inference phase. Fig. 3a displays an example of molecular generation, in which new molec-

a Molecular generation



b Target tracing

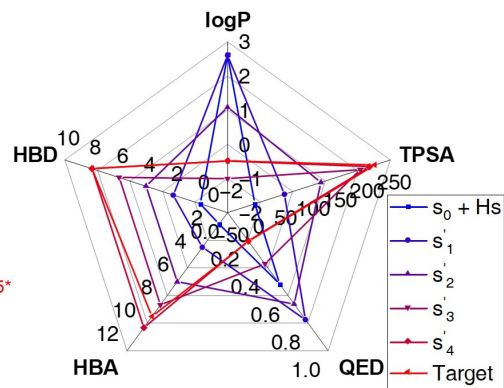


Fig. 3 Inference process for molecular generation. (a) An example of a molecular generation process. (b) Property changes for generated molecules.

ular fragments are selected and combined to complete a target molecule from steps 0 to 3. In the process, the properties of the generated potential output molecules (s_1 to s_4), which are derived from hydrogen attachment of the combined molecules (s_1 to s_4), change from the properties of hydrogen attached initial fragment ($s_0 + Hs$) to the target properties (logP: -0.488 , TPSA: 220.83, QED: 0.207, HBA: 9, HBD: 8). In step 3, the properties of the potential output molecule s_4 (logP: -0.488 , TPSA: 211.09, QED: 0.205, HBA: 10, HBD: 8) are close to the target properties (Fig. 3b). Since the target error ϵ_4 is lower than the maximum target error ϵ_{max} , the process is early terminated at step 3. Hence, the potential output molecule at step 3 (s_4) becomes the final output molecule.

2.3 Materials extrapolation to hit multiple extreme target properties

In this section, we empirically demonstrate that RL-guided combinatorial chemistry enables the discovery of extrapolated compounds, which is not possible with probability distribution-learning models. To achieve this, we adopt two different types of probability distribution-learning models and compare their performance with our model in terms of materials extrapolation. One of the adopted models is a conditional recurrent neural network (cRNN)²⁴. It serves as an NMT-based translator, translating input target properties into the corresponding molecular chemical language. As it operates as a translator, the input target properties and the corresponding molecular chemical language are one-to-one matched. The other model is the generative chemical Transformer (GCT)²³, a cVAE-based generative model. It utilizes the Transformer’s architecture as the backbone and incorporates a conditional latent space between its encoder and decoder. GCT generates chemical language corresponding to input target properties and sampled noise. As it functions as a generator using randomly sampled noise, it generates various molecular chemical languages with a single set of target properties.

For the demonstration, we conducted experiments on generating molecules to hit multiple target properties. The experimental setup was borrowed from ref.²⁴. In the experiments, the follow-

Table 1 The target-hitting errors for materials interpolation

	$RMSE_i$		\overline{RMSE}_i^a
	cRNN ²⁴	GCT ²³	Average
logP	0.379	0.368	0.373
TPSA	5.476	5.109	5.292
QED	0.081	0.075	0.078
HBA	0.932	1.204	1.068
HBD	0.223	0.247	0.235
MW	5.954	8.272	7.113
DRD2	0.113	0.098	0.105

^a \overline{RMSE}_i refers average $RMSE$ of target property $i \in \{\log P, TPSA, QED, HBA, HBD, MW, DRD2\}$ for cRNN²⁴ and GCT²³.

ing seven drug-related target properties were given to the models to generate target-hitting molecules: logP, TPSA, QED, HBA, HBD, MW, and DRD2. This experiment falls under Task type A as specified in Fig.2c. Since ϵ has multiple terms to minimize and multiple constraints, this toy problem covers complex optimization problems. By even changing the signs of some terms of ϵ , it is possible to cover complex optimization problems that involve a mix of minimization and maximization. Detailed information about the properties is summarized in Methods. Here, RDKit and a QSAR model for DRD2²⁴ were adopted as evaluators.

First, the original performances of cRNN²⁴ and GCT²³ in interpolation points were evaluated (Table 2). The two models were trained and tested with datasets²⁴ curated from the ChEMBL database²⁰. Here, how well target-hitting molecules were generated for the given target properties—which were gathered from 149,679 molecules in the curated ChEMBL test data²⁴—was evaluated. In contrast to the two methodologies, the proposed RL-CC approach in this paper requires retraining for each set of target properties. This makes it impractical for a realistic performance comparison in terms of interpolation, as training needs to be conducted individually for 149,679 properties. Additionally, RL-CC focuses on generating molecules with extreme properties, and thus, model performance in interpolation was not assessed for

RL-CC.

To conduct the experiments on materials extrapolation, we adopted another molecular dataset with properties that were more widely distributed than the trained data²⁴: PubChem SARS-CoV-2 clinical trials⁵⁰ (Fig. 4). Among the molecules in this dataset, 10 molecules were sampled whose properties were outside the trained data, which were then set as the extrapolated targets (C1 to C10). Since these 10 molecules were real molecules that exist in the real world, their properties would be physically feasible targets to generate. For each extrapolated target, 10,000 molecular generations were tried with cRNN²⁴ and GCT²³.

To evaluate the performance of generating molecules that hit multiple target properties, the criteria for determining whether each target property was hit should be defined. Accordingly, in the experiment of materials interpolation with cRNN²⁴ and GCT²³, the root mean squared error of each target property i ($RMSE_i$) was analyzed (Table 1). Since all $RMSE_i$ for cRNN and GCT were not significantly different from each other, we determined that the magnitude of the average $RMSE_i$ ($\overline{RMSE_i}$) represents the difficulty of generating molecules that hit the target property i . Therefore, by setting $target\ i \pm \overline{RMSE_i}$ as the target bound of i , a wide bound was assigned to targets that were difficult to hit and a narrow bound was assigned to any targets that were easy to hit. In this context, the term 'target-hitting molecule' refers to molecules with properties that fall within the range of $\pm \overline{RMSE_i}$ from the target values for each property.

Table 2 shows the results for materials interpolation. In Table 2, the results of interpolation for a total of 149,679 target properties were rescaled to 10,000 for comparison with the extrapolation results. Since the number of attempted molecular generations for materials interpolation and extrapolation were different, the rescaled results based on 10,000 trials are summarized in Table 2 for comparison. For materials interpolation, the cRNN²⁴ generated 2,948 molecules that hit all of the seven targets (logP, TPSA, QED, HBA, HBD, MW, and DRD2) simultaneously and 3,774 molecules hit the five targets (logP, TPSA, QED, HBA, and HBD) simultaneously. With the same criteria, the GCT²³ generated 2,321 molecules that hit all seven targets and 3,480 molecules hit the five targets simultaneously. These results confirmed that both models are able to generate target-hitting molecules in the trained region.

Results for materials extrapolation are shown in Table 3 and Fig. 5. According to the results, both probability distribution-learning models achieved poor results in terms of molecular extrapolation. For each target from C1 to C10 outside the trained data, we conducted 10,000 trials to generate the molecules per target. As shown in the results for the targets C1 to C10 of Table 3 and Fig. 5, both probability distribution-learning models failed to generate molecules that hit all of the targets and did not generate molecules that hit the five targets. GCT²³ only succeeded in generating seven valid and unique molecules that satisfied the chemical valence rule out of 100,000 trials, with four and three molecules being generated for targets C1 and C3, respectively. cRNN²⁴ generated a total of 15,068 chemically valid molecules, although only 21 were unique. In particular, 15,054 out of the 15,068 valid molecules were nonsensical outcomes

that were overlapped and too small, such as CH_4 , CH_4S , H_2O , H_2S , SO , H_2OS , and H_2S_2 . The MWs of these small molecules range from 16 and 66 *Da*. Considering that the target MWs of C1 to C10 ranged from 1,026 to 3,124 *Da*, it was difficult to conclude whether it operated correctly. Moreover, other generated molecules exhibited considerable deviations from the intended targets. Detailed information on the generated molecules is summarized in Table S1–S4†.

For the targets C1, C2, C3, C4, and C6, our RL-guided combinatorial chemistry generated a total of 1,315 target-hitting molecules that hit all seven targets simultaneously. Here, 355, 366, 233, 50, and 311 molecules that hit all targets were generated for targets C1, C2, C3, C4, and C6, respectively. For targets C5, C7, C8, C9, and C10, RL-guided combinatorial chemistry could not generate molecules that hit all seven target properties. However, it successfully generated a total of 828 molecules that hit five target properties that failed with the probability distribution-learning models. Here, 14, 321, 181, 289, and 23 molecules that hit five targets were generated for targets C5, C7, C8, C9, and C10, respectively.

Also, in fact, it is hard to assert that it completely failed to hit the seven target properties simultaneously for the targets C5, C7, C8, C9, and C10. For these targets, the generated molecules exhibited low target-hitting errors. This means that if the target bounds were more broadly set, there would be more molecules that were counted as molecules that hit all targets. It should be noted that the employed MW target bound ± 7.113 *Da* and DRD2 target bound ± 0.105 were fairly narrow (See Table 1). The target bound of MW 7.113 *Da* was so small that it was less than the weight of a single atom. Furthermore, the target bound of DRD2 0.105 was considerably smaller than the commonly known drug activity prediction accuracy of QSAR models. In ref.²⁴, the QSAR model for DRD2 was used as a binary classifier to evaluate as either active (when the predicted value was > 0.5) or inactive (≤ 0.5). For this reason, we believe that the number of molecules hitting the targets MW and DRD2 was less counted than the number of molecules hitting the other targets (See MW-column and DRD2-column of RL-CC in Table 3). Hence, we conducted a supplementary experiment on another dataset to generate five target-hitting molecules, excluding MW and DRD2 (ESI† Note 1). As a result, we confirmed that our model successfully generated molecules with extreme properties outside the known domain, which is not possible with probability distribution-learning models.

Moreover, RL-CC uses a selective binding approach within combinable molecular fragments based on the BRICS fragment combination rules. As a result, all generated molecules adhered to the chemical valence constraints, ensuring a 100% chemically valid. Furthermore, even when extreme target properties were specified, the diversity of chemically valid generated molecules remained remarkably high as seen in Fig. 5.

When choosing the molecular candidates, it is also important to consider the synthesizability of the generated molecules. Thus, we have analyzed the synthetic accessibility (SA) score of the generated molecules using RDKit, which represents the ease of chemical compounds to be synthesized or produced. SA score is eval-

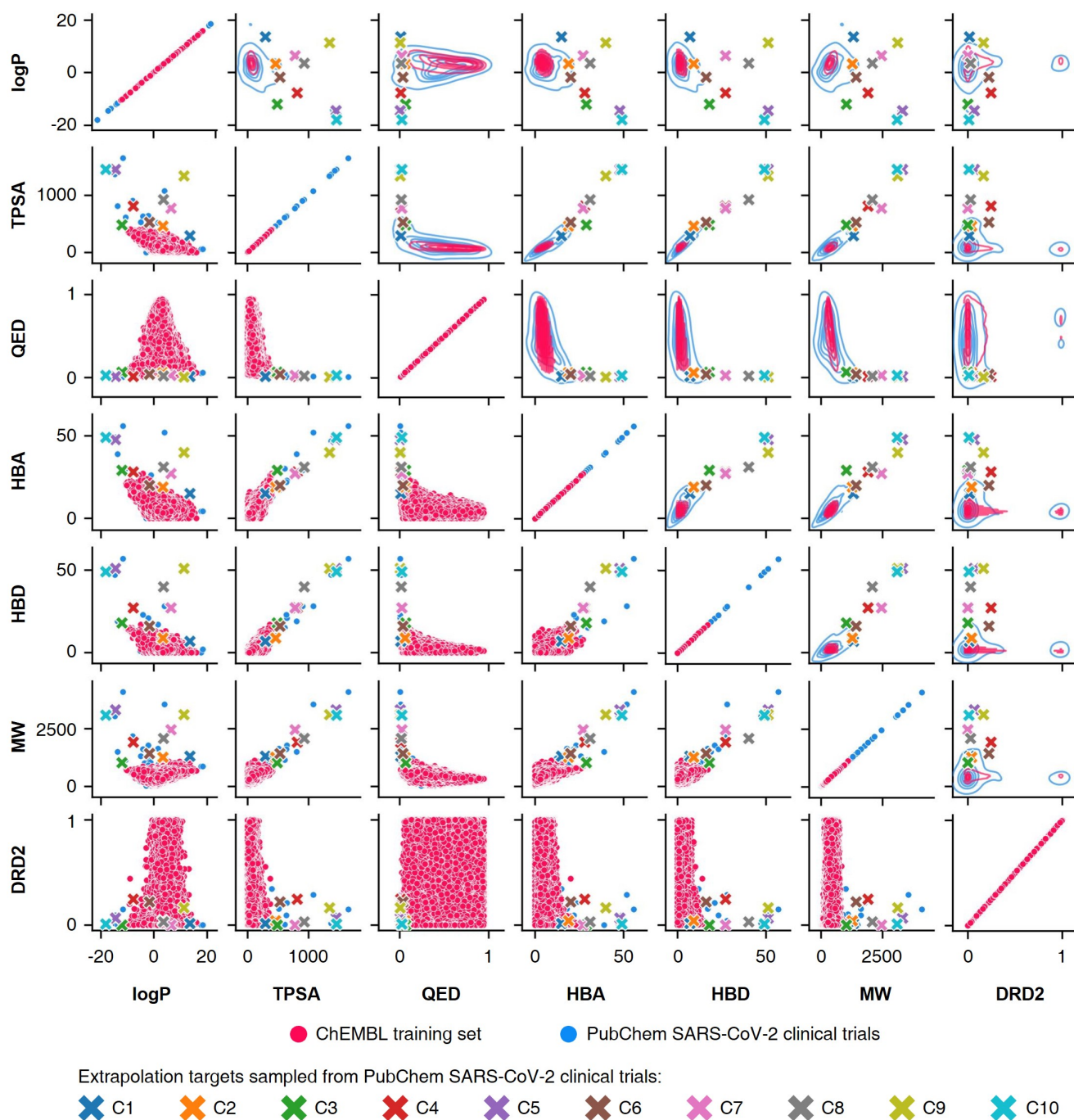


Fig. 4 Targets for materials extrapolation. The PubChem SARS-CoV-2 clinical trials dataset⁵⁰ is more widely distributed than the ChEMBL training dataset²⁰. The properties of five molecules in PubChem SARS-CoV clinical trials that deviated from the logP-TPSA distribution of the ChEMBL training dataset were set as extrapolation targets C1 to C5, and the properties of five molecules that deviated from the TPSA-QED distribution were set as extrapolation targets C6 to C10.

uated by considering how common the fragments composing the molecule are and the complexity of intricate ring structures such as fused rings. The SA scores for the generated molecules are presented in Figure S6†. The calculated results indicate that the generated molecules consistently exhibit low SA scores, excluding cases with extremely high molecular weights as seen in the experiment for generating molecules with extreme target properties. This suggests a reasonable level of synthesizability for the

generated molecules.

2.4 Application to the discovery of protein docking molecules

The discovery of small molecules that dock to a target protein is a practical problem in drug discovery. Moreover, binding affinity to a target receptor is an important indicator for measuring drug-

Table 2 Performance benchmark for materials interpolation

Model	# of valid mols. (# of unique mols.)	# of all target-hitting mols. w/o MW & DRD2 (# of unique mols.)	# of all target-hitting mols. (# of unique mols.)	# of each target-hitting mols.						
				logP	TPSA	QED	HBA	HBD	MW	DRD2
cRNN ²⁴	8475 (8475)	3774 (3774)	2948 (2948)	6263	6459	6653	7627	8077	6897	7796
GCT ²³	8715 (8715)	3480 (3436)	2321 (2290)	6289	6916	6693	7013	8200	5890	8114

Table 3 Performance benchmark for materials extrapolation

Model	Extrapolated targets	# of valid mols. (# of unique mols.)	# of all target-hitting mols. w/o MW & DRD2 (# of unique mols.)	# of all target-hitting mols. (# of unique mols.)	# of each target-hitting mols.						
					logP	TPSA	QED	HBA	HBD	MW	DRD2
RL-CC (This work)	C10	10000 (9999)	23 (23)	0 (0)	820	1133	9978	5533	2618	0	35
	C9	10000 (10000)	289 (289)	0 (0)	3919	1432	9995	7880	3223	1	15
	C8	10000 (9998)	181 (181)	0 (0)	2999	974	9992	6273	2379	466	133
	C7	10000 (9996)	321 (321)	0 (0)	3686	1420	9971	7832	3588	531	28
	C6	10000 (9981)	1709 (1708)	311 (311)	3769	3450	9890	8636	7301	1445	8729
	C5	10000 (10000)	14 (14)	0 (0)	1607	1377	9981	7381	2363	0	26
	C4	10000 (9969)	439 (439)	50 (50)	1972	1452	9809	7283	4384	572	9493
	C3	10000 (9869)	913 (877)	233 (224)	3143	2296	9940	8392	7143	1128	8310
	C2	10000 (9987)	2424 (2424)	366 (366)	6738	3145	9928	8415	8635	1388	4970
	C1	10000 (9994)	1317 (1317)	355 (355)	5202	2282	9918	9347	8622	1849	9406
cRNN ²⁴	C10	422 (2)	0 (0)	0 (0)	0	0	0	0	0	0	422
	C9	0 (0)	0 (0)	0 (0)	0	0	0	0	0	0	0
	C8	0 (0)	0 (0)	0 (0)	0	0	0	0	0	0	0
	C7	0 (0)	0 (0)	0 (0)	0	0	0	0	0	0	0
	C6	6 (6)	0 (0)	0 (0)	0	0	6	1	0	0	5
	C5	0 (0)	0 (0)	0 (0)	0	0	0	0	0	0	0
	C4	9836 (1)	0 (0)	0 (0)	0	0	0	0	0	0	0
	C3	3022 (5)	0 (0)	0 (0)	0	0	4	2	1	0	3022
	C2	0 (0)	0 (0)	0 (0)	0	0	0	0	0	0	0
	C1	1788 (10)	0 (0)	0 (0)	0	0	4	1	1	0	1788
GCT ²³	C10	0 (0)	0 (0)	0 (0)	0	0	0	0	0	0	0
	C9	0 (0)	0 (0)	0 (0)	0	0	0	0	0	0	0
	C8	0 (0)	0 (0)	0 (0)	0	0	0	0	0	0	0
	C7	0 (0)	0 (0)	0 (0)	0	0	0	0	0	0	0
	C6	0 (0)	0 (0)	0 (0)	0	0	0	0	0	0	0
	C5	0 (0)	0 (0)	0 (0)	0	0	0	0	0	0	0
	C4	0 (0)	0 (0)	0 (0)	0	0	0	0	0	0	0
	C3	3 (3)	0 (0)	0 (0)	0	0	3	1	0	0	3
	C2	0 (0)	0 (0)	0 (0)	0	0	0	0	0	0	0
	C1	4 (4)	0 (0)	0 (0)	0	0	1	0	0	0	4

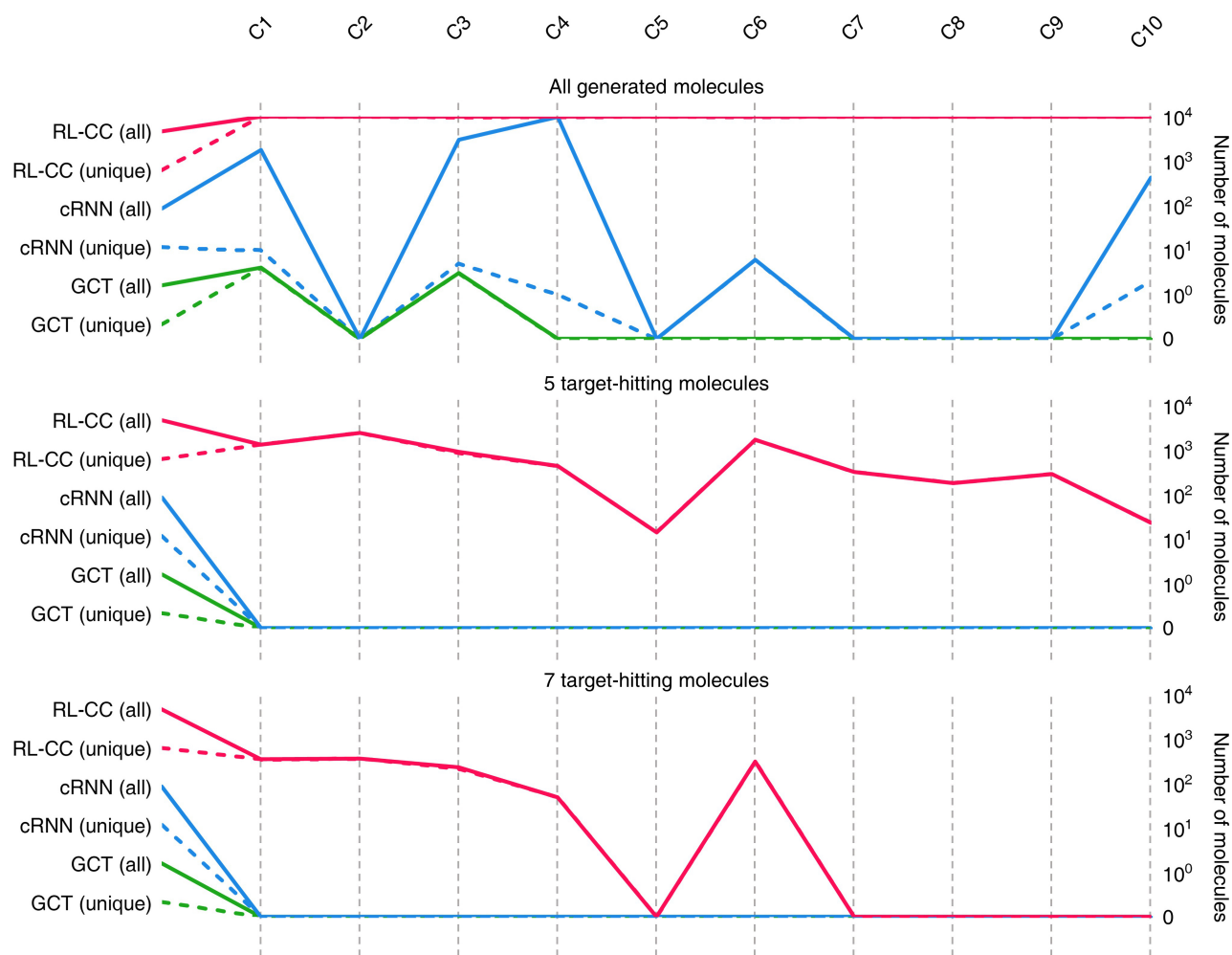


Fig. 5 Quality benchmarks of generated molecules in materials extrapolation. Number of chemically valid molecules, 5 target-hitting molecules (logP, TPSA, QED, HBA, and HBD), and 7 target-hitting molecules (logP, TPSA, QED, HBA, HBD, MW, and DRD2) out of 10,000 molecules produced for target C1 to C10. A solid line indicates the total number of valid molecules meeting each condition, and a short-dashed line shows the number of unique valid molecules (excluding overlaps).

target interactions³. Since molecules with higher binding affinity to the target protein (compared to other proteins) can be considered as having high selectivity and docking ability, the discovery of molecules that maximize target binding affinity is a key objective in protein docking drug discovery⁵¹. Therefore, to generate molecules with a low docking score, which means to generate molecules that can bind strongly with 5-HT_{1B} in this case, the trained policy attaches fragments that can maximize the reward.

In this section, we demonstrate that RL-guided combinatorial chemistry can discover molecules that maximize the binding affinity towards the 5-hydroxytryptamine receptor 1B (5-HT_{1B} receptor), which is related to mental diseases. A detailed description of the 5-HT_{1B} receptor is summarized in Methods. We adopted QVina2⁴⁸ (a data-free molecular docking simulator) to discover the minimum-energy docking conformation. This simulator evaluates the docking score quickly and reliably. Since the docking score is an indicator that is inversely proportional to the binding affinity, the reward function was set as the negative docking score.

To evaluate the performance of RL-guided combinatorial chemistry, the docking scores of 10,000 generated molecules from our model were compared with the docking scores of two other molecular sets. One was a set of 1,871 molecules that were generated to maximize the negative docking score towards the 5-HT_{1B} receptor using fragment-based generative RL with explorative experience replay for drug design (FREED)², which is reported in the paper. The other set was 10,000 molecules that were randomly sampled from ChEMBL²⁰ drug-like molecules. The docking scores of the three sets are summarized in Fig. 6a, which were calculated with QVina2. The calculation configuration is described in ESI† Note 4. The best molecule with the lowest docking score was discovered from our model and the median docking score for the sets was also the lowest. The top 10 generated molecular structures with the highest pIC₅₀ for CCR5, INT, and RT are illustrated in Fig. S8–S10†.

To check if potential drug molecules were found among the 10,000 generated molecules, we investigated whether any

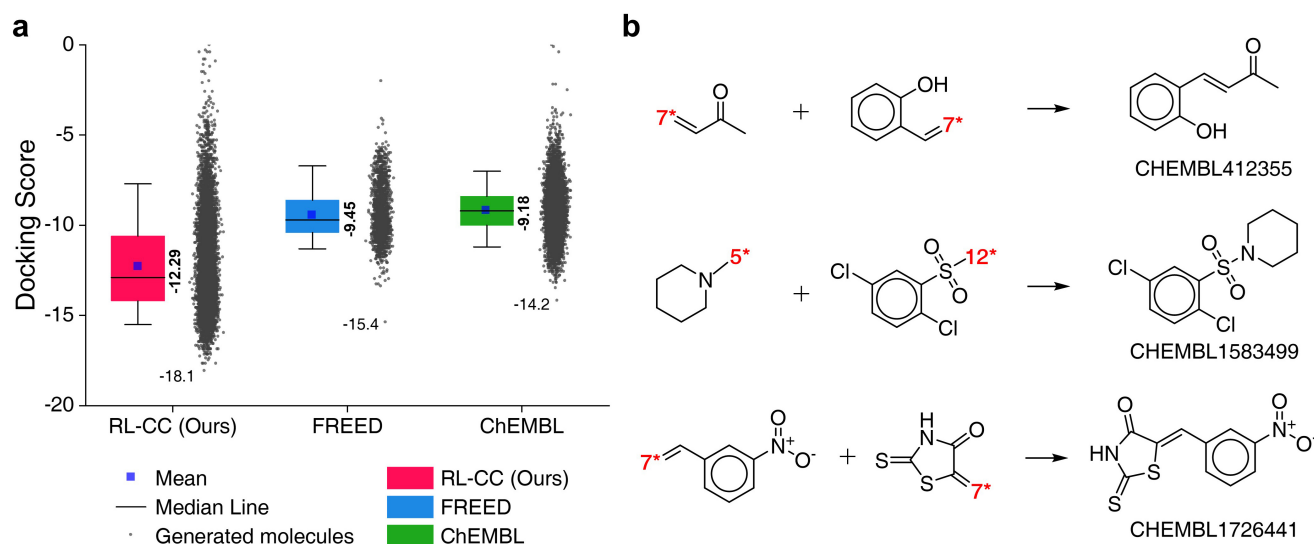


Fig. 6 Generated 5-HT_{1B} receptor docking materials. (a) Comparison of docking scores for the three molecular sets. Pink indicates the docking scores of 10,000 generated molecules from RL-guided combinatorial chemistry. Green indicates the docking scores of 10,000 drug-like molecules that were randomly sampled from ChEMBL²⁰ database. Blue indicates the docking scores of 1,871 molecules generated by FREED². The 1,871 molecules have been reported as de novo cases with 4-step in the paper. It should be noted that the maximum number of fragments constituting a compound was the same as ours. The docking scores of the 1,871 molecules were re-evaluated using QVina2⁴⁸ under the same calculation configuration as ours. The mean and minimum docking score for each outcome are represented numerically, while the box is set with percentiles 25 and 75, and the whiskers extend to the 5th and 95th percentiles. (b) Three molecular examples that were generated by RL-guided combinatorial chemistry, which exactly matched with active drug molecules reported in the PubChem Bioassay database⁵².

generated molecules were an exact match with the drug-like molecules in the ChEMBL²⁰ database. There were 23 molecules whose molecular structures exactly matched with real drug-like molecules in the ChEMBL database, of which 13 out of the 23 molecules had labels on drug activity (active or inactive). It should be noted that ref.⁴⁰ roughly estimated the number of small organic molecules as 10^{60} , of which only 2.2×10^6 were included in the ChEMBL database²⁰. Hence, it was difficult to find molecules with an exact match. An interesting finding is that five (CHEMBL1583499, CHEMBL1726441, CHEMBL412355, CHEMBL2261013, and CHEMBL99068) of the 13 molecules had been reported as active for some targets. Among these, three (CHEMBL1583499, CHEMBL1726441, and CHEMBL412355) were active in the related roles in which the 5-HT_{1B} docking molecules have been reported to have an effect. For example, CHEMBL1726441 is reported to be active for various targets such as Corticotropin-releasing factor receptor 2, Rap guanine nucleotide exchange factor 4, Nuclear factor erythroid 2-related factor 2, and Geminin. These targets have been reported to act in the human brain and peripheral tissues, playing a psychopathological role⁵³ and controlling brain function⁵⁴. These investigations were conducted with the PubChem Bioassay database⁵². The other investigated results for the two remaining molecules (CHEMBL2261013 and CHEMBL99068) are summarized in Table S7†.

2.5 Application to discovery of HIV inhibitors

This section describes experiments in which RL-guided combinatorial chemistry was applied to discover HIV inhibitors. Here,

we selected three HIV inhibition targets: C-C chemokine receptor type 5 (CCR5), HIV integrase (INT), and HIV reverse transcriptase (RT). Detailed information about the targets is summarized in Methods. To evaluate the HIV inhibition potency of molecules, pIC₅₀ predictors⁴ for the three HIV inhibition targets were adopted. It should be noted that pIC₅₀ is equal to $-\log_{10} IC_{50}$, where IC₅₀ is an indicator that measures the amount of a particular inhibitory substance required to inhibit a given biological process or biological component by 50%. In other words, the lower the value of IC₅₀, the higher the HIV inhibition potency. Moreover, the higher the value of pIC₅₀, the higher the HIV inhibition potency. Therefore, we set pIC₅₀ as the reward function to make our model discover HIV inhibitors with high potency.

In total, 10,000 generated molecules from our model were compared with the same number of molecules randomly combined by no-policy combinatorial chemistry (Fig. 7a). For all the HIV inhibition targets, molecules generated by our model exhibited significantly higher pIC₅₀ values compared to those of random combination without a policy (original combinatorial chemistry). This result indicated that our model learned the fragment-selection policy to discover the intended substances. The benchmark results compared to the other four generators for HIV inhibitors are summarized in Table S9†, in which our model achieved the highest pIC₅₀ values for targets CCR5 and RT. The top 10 generated molecular structures with the lowest docking score are illustrated in Fig. S7†.

To analyze the policy change of molecular fragment selection in the training phase, we generated 10,000 molecules at the end of every training iteration. The derived frequencies (how many

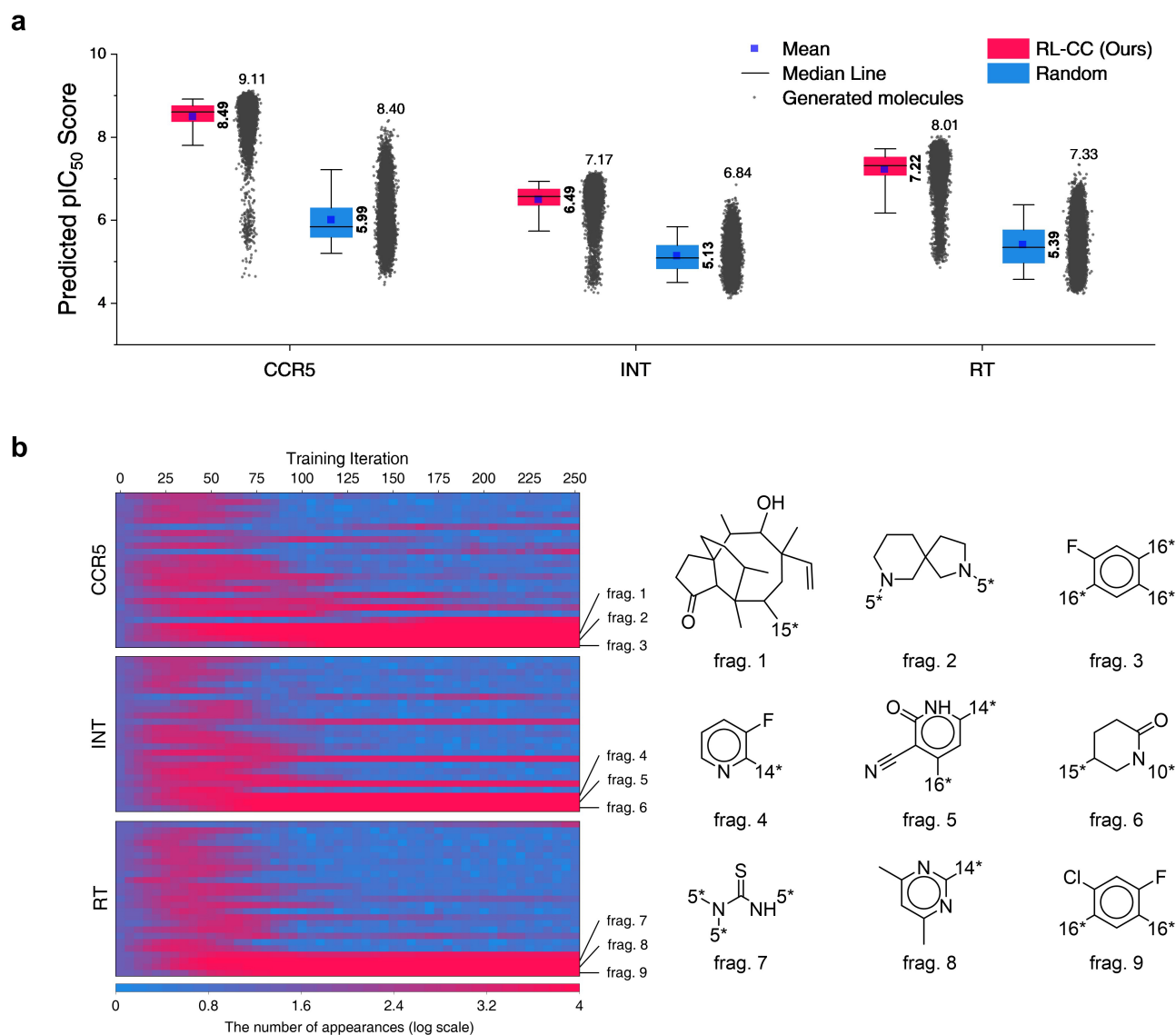


Fig. 7 Results for HIV inhibitors discovery with high pIC_{50} for three HIV inhibition targets: CCR5, INT, and RT. (a) Comparison of pIC_{50} for two molecular sets. Pink indicates pIC_{50} for a set of 10,000 molecules generated by RL-guided combinatorial chemistry. Blue indicates pIC_{50} for a set of 10,000 drug-like molecules that were randomly sampled from the ChEMBL database²⁰. The mean and maximum pIC_{50} values for each outcome are represented numerically, while the box is set with percentiles 25 and 75, and the whiskers extend to the 5th and 95th percentiles. (b) Policy changes in BRICS molecular fragment selection according to the training steps. The left-hand side of the figure shows the number of appearances for 25 molecular fragments with the biggest change. The vertical and horizontal axes of the left-hand side blue-red plot represent the type of fragment and the training iteration, respectively. Blue-red indicates the number of generated molecules that have the fragment among the 10,000 generated molecules.

molecules had the fragment) for 25 fragments with the biggest change are plotted on the left of Fig. 7b. In the initial state (where no policy was learned), the frequency of all fragments was similar. As the training progressed, the frequency of each fragment became varied. Although the selected frequency of some fragments increased as training proceeded, some of them decreased at certain points. This is because the agent found the combinations of molecular fragments that provided a high reward. Hence, the selection of other fragments that did not have any merit in the pIC_{50} score rapidly decreased. The most selected fragments differed according to the type of HIV inhibition targets. Since the fragments were most often used to maximize the pIC_{50} for each

target, we hypothesize that they may be key structures for HIV inhibitors on each target.

2.6 Expansion potential for discovery of organic materials

Fig. 8a,b illustrate the results of fragmenting TADF emitters for single-layer OLED by leveraging the BRICS fragment combination rules in reverse. Examination of the fragments depicted in Fig. 8a reveals that by inversely applying the BRICS fragment combination rules, it is possible to fragment the emitter into acceptor, donor, and bridge components, aligning with the knowledge of designing photoactive materials. However, the emitter shown in

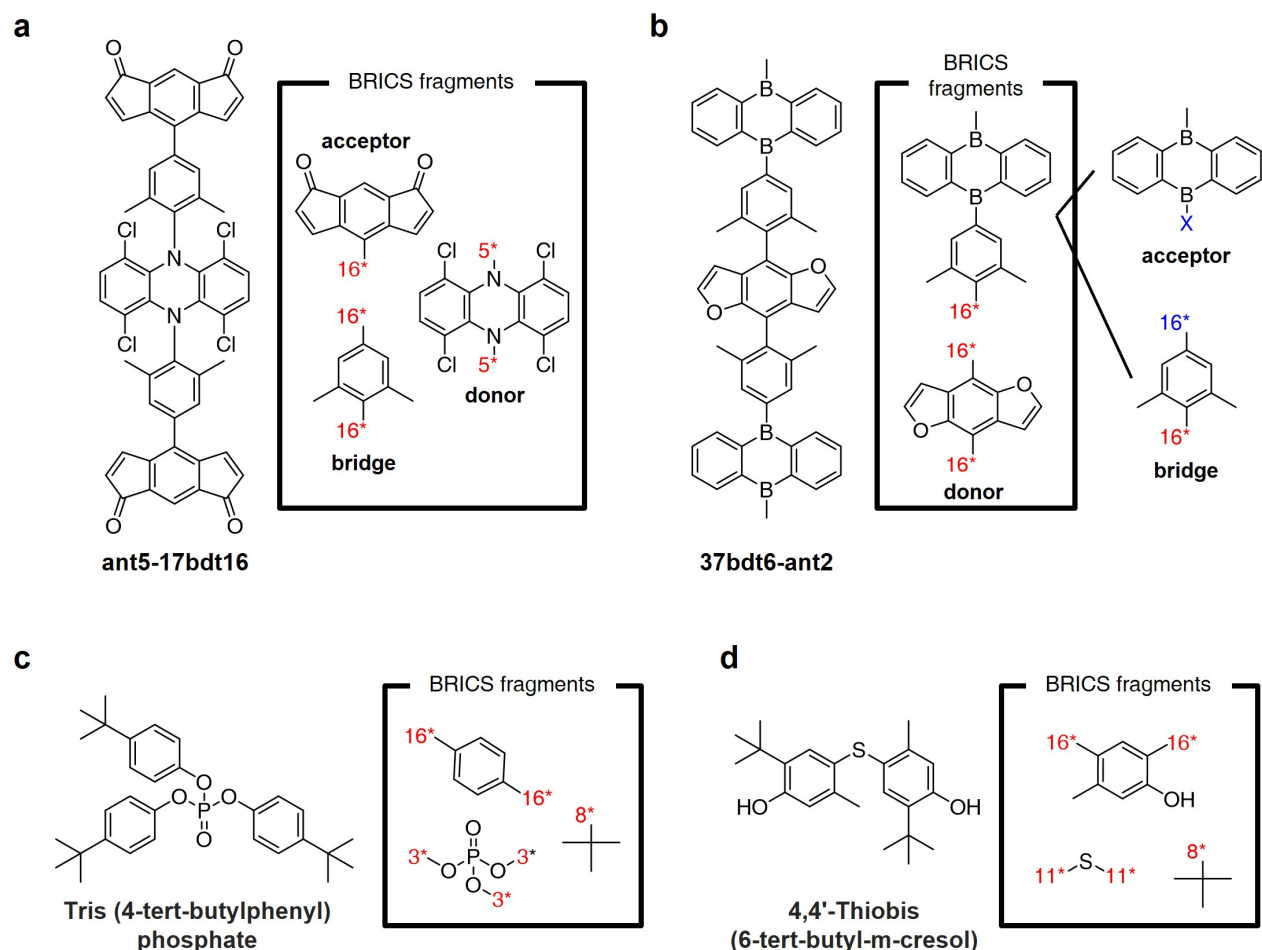


Fig. 8 BRICS fragmentation of organic materials. (a,b) Thermally-activated delayed fluorescence (TADF) emitters for single-layer OLED reported in ref.⁵⁵. (c,d) Flame retardant materials reported in ref.⁵⁶.

Fig. 8b displays a chunk where the combination of acceptor and bridge remains undivided. This occurrence is due to the BRICS rules covering only the bonds between C, N, O, and S elements, lacking rules for bonds at the B-X binding sites marked in blue in Fig. 8b. Consequently, this highlights a limitation that for the BRICS rules to encompass a wider range of organic materials beyond drugs, there is a need to incorporate additional rules for various elemental bonds. Fig. 8c,d show the fragmentation results of organic flame retardant materials using the BRICS fragment combination rules in reverse. These results indicate that if the BRICS fragment combination rules are well-expanded and inversely applied to construct the fragment set of targeted materials, RL-CC has the potential to be sufficiently extended to the discovery of organic materials.

3 Conclusion

From a data science perspective, the discovery of better than previously known is to find new substances with properties outside outliers. In particular, research on inverse molecular design models with extrapolated target properties can be considered as fundamental groundwork for materials extrapolation. Most of the reported inverse molecular design models are based on

data probability distribution-learning models, such as machine translators and generative models (including Seq2Seq²⁵, Transformer²⁶, GAN²⁹, and VAE³⁰). However, these models are too limited for use in materials extrapolation, which requires discovering substances in the untrained area. To solve this problem, we adopted combinatorial chemistry³⁸, which generates molecules from combinations of randomly selected molecular fragments. Fundamentally, it is a rule-based molecular designer for generating all chemically possible molecular structures that can be obtained from the combination of molecular fragments. However, since the lack of a molecular fragment selection policy can cause a combinatorial explosion⁴¹, RL is applied to train its fragment-selection policy to provide a direction toward target substances.

This paper contains three major contributions. First, we theoretically demonstrated that most inverse molecular design models based on probability distribution-learning of data are too limited for use in materials extrapolation. Second, we empirically demonstrated that our proposed RL-guided combinatorial chemistry works well on various discovery problems with extreme/extrapolated properties, such as the discovery of multiple target-hitting molecules, protein docking molecules, and HIV inhibitors. Since the BRICS³⁹ system is designed based on drug-like

molecules, our applications were limited to the discovery of drug molecules. For these reasons, we have shown the feasibility of applying the proposed methodology to the discovery of organic materials by using the BRICS fragment bonding rules in reverse to decompose molecules of organic materials. This also highlights the limitations of the BRICS fragment combination rules that need to be addressed in order to further extend the scope of materials discovery. The problems addressed in this study exhibit significant overlap with practical materials discovery issues. For instance, photoactive materials used in applications such as organic light-emitting displays, solar cells, optical sensors, bio-electronic devices, and liquid crystal displays are compounds designed through combinations of molecular fragments. The common goals of these photoactive materials discovery are finding new and better materials that satisfy target properties, such as the energies of the S₀, S₁, T₁ states, and their gaps. Additionally, considerations for band gaps in semiconductors and transport properties in battery electrolytes fall within these kinds of problems. Third, the limitations of our model were also analyzed in Methods. One of these was that re-training would be required to discover multiple target-hitting molecules if the targets were changed. The other limitation was a sparse reward problem that interrupted the discovery of materials with extreme properties. However, ongoing research efforts aimed at addressing these limitations suggest that they can be resolved through future studies.

4 Methods

4.1 Molecular Descriptors

For the experiment in materials extrapolation, where the aim was to hit multiple extreme target properties, seven properties were set: logarithm of the calculated octanol-water partition coefficient (logP)⁴⁵; topological polar surface area (TPSA)⁴⁶; quantitative estimate of drug-likeness (QED)⁴⁷; number of hydrogen bond acceptors (HBA); number of hydrogen bond donors (HBD); molecular weight (MW); and drug activity for dopamine receptor D2 (DRD2). Each property is considered important in the field of drug discovery. The term logP is a descriptor for the lipophilicity of a molecule, which refers to a molecule's capacity to dissolve in fats or oils. This is an important property in drug design since it has an impact on the molecule's capacity for penetrating cell membranes and reaching its intended target. The term TPSA is a calculated descriptor of the polar surface area (PSA) of a molecule, which refers to the area of a molecule having polar functional groups that could form hydrogen bonds with water molecules. A molecule is less polar and more likely to be able to penetrate cell membranes if it has a lower PSA value. The terms HBA and HBD are also important properties in drug design because they can affect a molecule's capacity to interact with other molecules through hydrogen bonding. Hydrogen bonding is frequently used in drug design to facilitate the binding of a molecule to the target receptor. Moreover, hydrogen bonding can affect a drug molecule's solubility and permeability, which influence its pharmacological properties. Term MW is a descriptor used in drug discovery, as it can affect a drug's pharmacokinetics, efficacy, and safety. This is because the size of the molecules can influence

a drug's absorption, distribution, metabolism, or degree of penetration into the cell membrane. The correct molecular weight of a drug depends on its application. However, most drugs generally comprise small molecules with a molecular weight of less than 500 Da. This is because drug molecules have a higher likelihood of passing through a cell's membrane and have a lower likelihood of being affected by biometabolic reactions. The term QED is a metric used to evaluate a molecule's overall drug-likeness, which is a geometric mean of logP, HBA, HBD, PSA, number of rotatable bonds (ROTB), number of aromatic rings (AROM), and number of structural alerts (ALERTS). A molecule with a high QED value is more likely to be a promising drug candidate. Finally, DRD2 refers to a drug's activity toward dopamine receptor D2. The dopaminergic neurotransmission is regulated by the G protein-coupled receptor dopamine receptor D2, which is mainly expressed in the brain.

In the experiment aimed at discovering protein docking molecules, QVina2⁴⁸—a tool to discover the minimum-energy docking conformation and calculate its docking score—was employed to compute a docking score. This score is proportional to the binding strength between a drug molecule and its target. QVina2 calculates the docking score by simulating how a drug molecule interacts with a given target receptor in a three-dimensional simulation box. We targeted the protein receptor 5-HT_{1B}. Many studies have reported that activating 5-HT_{1B} receptors outside the brain has vascular effects (such as pulmonary vasoconstriction, which can help treat angina⁵⁷). Moreover, reduced 5-HT_{1B} heteroreceptor activity can increase impulsive behavior, whereas reduced 5-HT_{1B} autoreceptor activity can have an antidepressant-like effect^{58,59}.

In the experiment aimed at discovering HIV inhibitors, we selected three HIV-related targets: C-C chemokine receptor 5 (CCR5), HIV integrase (INT), and HIV reverse transcriptase (RT). Here, CCR5 is the immune system-related protein, which is found on the surface of white blood cells. Along with C-X-C chemokine receptor 4, it is a key co-receptor for HIV entry⁶⁰. The second target was INT, which is involved in viral replication and facilitates the viral cDNA's insertion into the infected cells¹. The final target was RT, which triggers the reverse transcription process. Here, the process can cause mutation and recombination that form the genetic diversity of HIV, enabling the formation of viral variants that could evade host immune responses, rendering the virus resistant to medication treatments⁶¹. For each target in the experiment, we tried to maximize its pIC₅₀ value, which is a descriptor for the potency of a drug in inhibiting a biological activity. It is calculated as the negative logarithm of the IC₅₀ value, which is the amount of a drug that inhibits 50% of the biological activity. In other words, the drug's potency increases as the IC₅₀ value decreases. In drug discovery, IC₅₀ is commonly utilized to compare the effectiveness of potential drug candidates.

4.2 Fragment set configuration

Two types of fragment sets were used in this study. One set contained 2,207 BRICS fragments that appeared more than 150 times in the training set²⁴ curated from the ChEMBL database²⁰

(release version 25). This fragment set was used for three major experiments: the discovery of seven target-hitting molecules, protein docking materials, and HIV inhibitors. For the supplementary experiment aimed at discovering five target-hitting molecules (ESI† Note 1), another fragment set containing 2,547 BRICS fragments that appeared more than 100 times in the training set of the MOSES database¹⁹ was used. The detailed reasoning for using these fragment sets is described in ESI† Note 2.

4.3 Action masking

For efficient learning, we applied action masking to our model (stage 2 in Fig. 2a). Based on the molecule in the current state, the list of actions that the agent can choose is limited by action masking. Since our model combines fragments according to BRICS fragment combination rules, the fragments that could not be connected to the molecule in the current state were masked. Thereby, more efficient learning was possible since the number of selectable actions in the current state was reduced, which improved the performance of our model (ESI† Note 3).

4.4 Target properties and calculation of molecular descriptors

In this study, three major experiments were conducted to generate molecules with extreme properties. In the first experiment, discovering molecules that could hit the multiple target properties was attempted. In the other experiments, discoveries of molecules that maximize interesting properties were attempted. Accordingly, the interesting properties could be calculated by the evaluators in the environment of the RL model. The detailed information on model accuracy can be found in ESI† Note 7.

For the first experiment on materials extrapolation to hit multiple extreme target properties, seven molecular descriptors were set as the targets: $\log P$ ⁴⁵, TPSA⁴⁶, QED⁴⁷, HBA, HBD, MW, and DRD2²⁴. Here, the DRD2 was calculated using a QSAR model for DRD2²⁴, while the other descriptors were calculated using RDKit⁴⁴. We selected 10 target sets of molecular properties out of known molecular data and attempted to generate the target-hitting molecules to demonstrate that our model would work well in terms of materials extrapolation. These 10 target sets of extreme properties were taken from an untrained dataset—PubChem SARS-CoV-2 clinical trials⁵⁰—whose molecular properties are more widely distributed than the training data set²⁴ (Fig. 4). Since the 10 target sets of extreme properties were taken from real molecules, they could be considered chemically feasible targets to discover.

For the experiment to discover protein docking materials, the calculated docking score between a docking molecule and 5-HT_{1B} protein receptor was set as the target. The docking score was calculated using QVina2⁴⁸, which calculates the docking score of a docking molecule by searching for its minimum-energy docking conformation. This program employs an empirical scoring function to predict the docking score, which includes several terms that incorporate various physical and chemical interactions between the ligand and protein. These interactions include van der Waals interactions, electrostatic interactions, hydrogen bonds,

and solvation effects. Moreover, QVina2 makes use of finely tuned scoring function parameters that are derived using many experimentally-identified ligand-protein complexes. It calculates a docking score for each docking posture it produces, with the lowest value being the most energetically favorable binding conformation. The detailed calculation configuration for QVina2 is illustrated in ESI† Note 4.

For the experiment to discover HIV inhibitors, the target property was set to maximize the pIC₅₀ score to three HIV-related targets: CCR5, INT, and RT. Each pIC₅₀ score was calculated by the light gradient boosting machine (LGBM)⁶²-based QSAR models² for the three HIV-related targets⁴. In addition, the QSAR model was trained to predict the pIC₅₀ value for each target using the ChEMBL dataset²⁰.

4.5 Training loop

To maximize the cumulative reward for sequential actions, RL trains its agent to learn which action to choose at each step. In this study, the action is a selection of a molecular fragment. The reward is the value calculated with the evaluator(s) by the experiment-specific reward function. By repeating this process, the policy that selects an action that can maximize the cumulative reward is gradually updated. After sufficient learning, the policy could then select sequential actions to generate a desired molecule that fits the given task.

The episode proceeds from steps 0 to T , where T is the designated maximum fragment number of the molecule. To generate diverse molecules, the first fragment is randomly selected. When selecting the next molecular fragment to be combined with the current molecule, action masking is conducted. In the process of action masking, the molecular fragments that cannot be combined with the current molecule are masked according to the BRICS fragmentation combination rules. Subsequently, the policy selects a molecular fragment from the unmasked fragments and binds it to an unfilled binding site. If the combined molecule still has any unfilled binding sites, hydrogen atoms are attached to derive a complete molecule and evaluate its properties of the current state. When a molecule that meets the set of criteria is generated, the fragment attachment is stopped and the episode ends early before reaching step T . Otherwise, the process is repeated during step T . After the final output molecule is generated, a reward for the episode is calculated depending on how closely the targets are hit. Since the reward is given only at the end of an episode, the policy undergoes updates aimed at achieving a global solution rather than a local one. By iteratively conducting the training episodes, the agent of RL learns a policy that maximizes the given reward function. The episode training is repeated until a preset number of training iterations is reached. For each experiment, the training iteration was set to 750, 80, and 250 times.

Training for a predefined number of iterations was conducted using an Intel Xeon Gold 6226R. For each experiment, it took 12, 140, and 30 hours, respectively. The variation in training times arises from differences in the time required for property prediction and the batch size used at each training iteration. For each experiment, it takes an average of 0.35, 0.7, and 15 seconds, re-

spectively, to predict the properties at each step. Additionally, the models’ accuracy can be found in ESI† Note 7 and Table S10†. For our model, retraining is required from scratch each time the target changes. Although transfer learning and other techniques for high efficiency may be considered in the future, they have not been applied as of now. In materials discovery, a fixed target is typically provided once the problem is given, enabling the training of the policy only once, and subsequent inference can be repeated at a low cost.

4.6 Rewards and terminations

In RL, it is important to have an appropriate set of termination conditions and target conditions to learn a decent policy. In all three experiments conducted in this study, there were two common termination conditions. First, molecular generation was terminated when the number of fragments that make up a compound in the current state n_{eval} exceeded the maximum number of fragments n_{max} , which was set to 50, 4, and 6 for each experiment. Second, the process was terminated when the number of unfilled binding sites n_L was equal to zero.

For the experiment on materials extrapolation to hit multiple extreme target properties, the process was terminated if the MW in the current state MW_{eval} exceeded the maximum MW ($MW_{max} = 3,500 Da$). Furthermore, it was also terminated if the error (ε) was less than the error threshold $\varepsilon_{th} = 0.05$. Here, ε was calculated as

$$\varepsilon = \sum_{y \in prop} \left(\frac{y_{trg} - y_{eval}}{\sigma_y} \right)^2 \quad (5)$$

where y_{trg} , y_{eval} , and σ_y denote the target y , evaluated y , and standard deviation of y for the curated ChEMBL training set²⁴, respectively. Here, *prop* is a set of properties that includes logP, TPSA, QED, HBA, HBD, MW, and DRD2.

The design of the reward function is also important since RL is performed based on the reward obtained by taking an action. Moreover, a penalty can be given to avoid any undesired actions. For the experiment on materials extrapolation to hit multiple extreme target properties, the reward function r was designed as follows:

$$r = \begin{cases} 0, & \text{if } \{[MW_{eval} < MW_{min}] \vee [n_{eval} < n_{min}]\} \wedge [n_L \neq 0], \\ -50, & \text{if } \{[MW_{eval} < MW_{min}] \vee [n_{eval} < n_{min}]\} \wedge [n_L = 0], \\ \frac{100}{\varepsilon+1}, & \text{else if } \varepsilon < \varepsilon_{th}, \\ \frac{30}{\varepsilon+1}, & \text{otherwise.} \end{cases} \quad (6)$$

Here, MW_{min} and n_{min} were set to generate various compounds by avoiding premature termination, which would generate uniform molecules that were too small. For this purpose, when the number of unfilled binding sites n_L was not equal to zero, a zero reward was given if MW_{eval} was less than MW_{min} or n_{eval} was less than n_{min} . When n_L was equal to zero, a reward of -50 was given if MW_{eval} was less than MW_{min} or n_{eval} was less than n_{min} . However, if a generated molecule did not correspond to the above two cases, a reward proportional to the degree of proximity to the target was awarded.

For the other two experiments (discovery of protein docking materials and HIV inhibitors), the reward function r was designed

as follows:

$$r = \begin{cases} 0, & \text{if } \{[MW_{eval} < MW_{min}] \vee [n_{eval} < n_{min}]\} \wedge [n_L \neq 0], \\ -50, & \text{if } \{[MW_{eval} < MW_{min}] \vee [n_{eval} < n_{min}]\} \wedge [n_L = 0], \\ pIC_{50}, & \text{otherwise.} \end{cases} \quad (7)$$

Here, the predicted score refers to the calculated docking and pIC_{50} scores of the HIV-related target, respectively.

4.7 RL algorithm

We performed benchmark testing against the following state-of-the-art RL algorithms: IMPALA⁶³, APPO⁶⁴, A2C & A3C⁶⁵, and PPO⁴⁹. The detailed results of the benchmarking are summarized in ESI† Note 3. From the benchmark results, we confirmed that PPO—which is a model-free, on-policy, actor-critic, and policy-gradient algorithm—was the most suitable for our problems, with a very large discrete action space of over 2,000. Moreover, PPO is known for its good performance, stability, and good sample efficiency, which makes the training process more stable by avoiding large policy updates with importance sampling and reusing learning data on the trust region. Hence, we applied PPO for all experiments conducted in this study. The objective function of PPO is defined as follows:

$$L^{CLIP}(\theta) = \hat{E}[\min(r_t(\theta)\hat{A}_t, clip(r_t(\theta), 1 - \varepsilon, 1 + \varepsilon)\hat{A}_t)], \quad (8)$$

where $r_t(\theta) = \frac{\pi_\theta(a_t | s_t)}{\pi_{\theta_{old}}(a_t | s_t)}$

where \hat{E}_t represents the expected value at time step t . Term r_t denotes the ratio between the new policy π_θ and the old policy $\pi_{\theta_{old}}$. The policy is expressed as $\pi_\theta(a_t | s_t)$, where a_t and s_t are the action and state at timestep t , respectively. In Equation (8), \hat{A}_t denotes the advantage function at time step t , which estimates the result of the step action more effectively than the behavior of the default policy.

4.8 Further findings

We empirically demonstrated that our methodology can discover novel molecules with extreme properties, which is impossible to accomplish with existing models that learn the probability distribution of data. However, there were two limitations with our model, which could be solved through further studies. First, the model should be re-trained if the target changes because the reward function depends on the given target. Therefore, the model must learn the policy from the start each time a new target is set. To solve this problem, a methodology such as meta-learning may be applied in future studies. With meta-learning, it is possible to predict the results of a new task or recommend hyperparameters based on the learning results from another task. Therefore, when a new task is assigned, it will be possible to learn through the experiences that have been taught in the past, requiring less additional training. For example, using methods such as Meta-GenRL⁶⁶, which applies meta-learning to reinforcement learning, the model outperformed the existing reinforcement learning algorithm while exhibiting similar performance for completely differ-

ent tasks. Second, there was a sparse reward problem, which occurred because the agent received little feedback or reward for the action from the environment, rendering it difficult to learn efficient policies and satisfy the desired goal. Since molecules with extreme properties are rarer than common molecules, the probability of experiencing an episode in which a rare molecule is obtained through a random combination of molecular fragments is relatively low. To solve this problem, we could adopt methods that encourage more exploration with curiosity. This would allow experiencing more episodes that could provide higher rewards. In addition, hierarchical reinforcement learning⁶⁷ could be applied, which is a methodology that utilizes prior knowledge of the given problem to set sub-goals that are easier to achieve than the original goal. Accordingly, it learns a policy that can achieve the original goal through policies learned from sub-goals.

Data availability

The curated ChEMBL datasets and MOSES data sets for training and testing cRNN²⁴ and GCT²³ are publically available at <https://github.com/MolecularAI/Deep-Drug-Coder> and <https://github.com/molecularsets/moses>, respectively. All generated molecules in this study are available at <https://github.com/Haeyeon-Choi/RL-CC/tree/main/result>.

Code availability

The full code used to perform the analysis is available at <https://github.com/Haeyeon-Choi/RL-CC>.

Author Contributions

HK proposed the concept of materials extrapolation and the scheme of RL-guided combinatorial chemistry. HK, HC, and JN designed the experiments, and they were implemented by HK, HC, and DK. All authors analyzed the results and discussed them. HK, HC, and DK wrote the manuscript, and all authors reviewed it. JN and WBL supervised the project.

Conflicts of interest

There are no conflicts to declare.

Acknowledgements

This research was supported by the National Research Foundation of Korea (NRF) grant funded by the Korean Government through the Ministry of Science and ICT (MSIT) (NRF-2021R1C1C1012031, NRF-2021R1A4A3025742, NRF-2018M3D1A1058633, and NRF-2020M3F7A1094299).

References

- 1 Y. Pommier, A. A. Johnson and C. Marchand, *Nature reviews Drug discovery*, 2005, **4**, 236–248.
- 2 S. Yang, D. Hwang, S. Lee, S. Ryu and S. J. Hwang, *Advances in Neural Information Processing Systems*, 2021, **34**, 7924–7936.
- 3 D. B. Kitchen, H. Decornez, J. R. Furr and J. Bajorath, *Nature reviews Drug discovery*, 2004, **3**, 935–949.
- 4 S. K. Gottipati, B. Sattarov, S. Niu, Y. Pathak, H. Wei, S. Liu, S. Blackburn, K. Thomas, C. Coley, J. Tang *et al.*, *International Conference on Machine Learning*, 2020, pp. 3668–3679.
- 5 A. Klein, C. Körber, A. Wachau, F. Säuberlich, Y. Gassenbauer, S. P. Harvey, D. E. Proffit and T. O. Mason, *Materials*, 2010, **3**, 4892–4914.
- 6 R. L. Greenaway and K. E. Jelfs, *Advanced Materials*, 2021, **33**, 2004831.
- 7 D. Sylvinson MR, H.-F. Chen, L. M. Martin, P. J. Saris and M. E. Thompson, *ACS applied materials & interfaces*, 2019, **11**, 5276–5288.
- 8 K. Kim, S. Kang, J. Yoo, Y. Kwon, Y. Nam, D. Lee, I. Kim, Y.-S. Choi, Y. Jung, S. Kim *et al.*, *npj Computational Materials*, 2018, **4**, 1–7.
- 9 B. Meredig, E. Antono, C. Church, M. Hutchinson, J. Ling, S. Paradiso, B. Blaiszik, I. Foster, B. Gibbons, J. Hattrick-Simpers *et al.*, *Molecular Systems Design & Engineering*, 2018, **3**, 819–825.
- 10 J. Ling, M. Hutchinson, E. Antono, S. Paradiso and B. Meredig, *Integrating Materials and Manufacturing Innovation*, 2017, **6**, 207–217.
- 11 E. O. Pyzer-Knapp, C. Suh, R. Gómez-Bombarelli, J. Aguilera-Iparraguirre and A. Aspuru-Guzik, *Annual Review of Materials Research*, 2015, **45**, 195–216.
- 12 J. Liu, S. Gong, H. Li and G. Liu, *Fuel*, 2022, **313**, 122712.
- 13 Y. Dan, Y. Zhao, X. Li, S. Li, M. Hu and J. Hu, *npj Computational Materials*, 2020, **6**, 1–7.
- 14 S. S. SV, J. N. Law, C. E. Tripp, D. Duplyakin, E. Skordilis, D. Biagioni, R. S. Paton and P. C. St John, *Nature Machine Intelligence*, 2022, 1–11.
- 15 Y. Dong, D. Li, C. Zhang, C. Wu, H. Wang, M. Xin, J. Cheng and J. Lin, *Carbon*, 2020, **169**, 9–16.
- 16 M.-Y. Lyu and T. G. Choi, *International journal of precision engineering and manufacturing*, 2015, **16**, 213–220.
- 17 R. Stauber, *ATZ worldwide*, 2007, **109**, 2–4.
- 18 A. Zunger, *Nature Reviews Chemistry*, 2018, **2**, 1–16.
- 19 D. Polykovskiy, A. Zhebrak, B. Sanchez-Lengeling, S. Golovanov, O. Tatanov, S. Belyaev, R. Kurbanov, A. Artamonov, V. Aladinskiy, M. Veselov *et al.*, *Frontiers in pharmacology*, 2020, **11**, 1931.
- 20 D. Mendez, A. Gaulton, A. P. Bento, J. Chambers, M. De Veij, E. Félix, M. P. Magariños, J. F. Mosquera, P. Mutowo, M. Nowotka *et al.*, *Nucleic acids research*, 2019, **47**, D930–D940.
- 21 O. Méndez-Lucio, B. Baillif, D.-A. Clevert, D. Rouquié and J. Wichard, *Nature communications*, 2020, **11**, 1–10.
- 22 J. Lim, S. Ryu, J. W. Kim and W. Y. Kim, *Journal of cheminformatics*, 2018, **10**, 1–9.
- 23 H. Kim, J. Na and W. B. Lee, *Journal of Chemical Information and Modeling*, 2021, **61**, 5804–5814.
- 24 P.-C. Kotsias, J. Arús-Pous, H. Chen, O. Engkvist, C. Tyrchan and E. J. Bjerrum, *Nature Machine Intelligence*, 2020, **2**, 254–265.
- 25 I. Sutskever, O. Vinyals and Q. V. Le, *Advances in Neural Information Processing Systems (NeurIPS)*, 2014.
- 26 A. Vaswani, N. Shazeer, N. Parmar, J. Uszkoreit, L. Jones, A. N.

- Gomez, Łukasz Kaiser and I. Polosukhin, *Advances in Neural Information Processing Systems (NeurIPS)*, 2017.
- 27 M. Mirza and S. Osindero, *arXiv preprint arXiv:1411.1784*, 2014.
 - 28 K. Sohn, H. Lee and X. Yan, *Advances in neural information processing systems*, 2015.
 - 29 I. Goodfellow, J. Pouget-Abadie, M. Mirza, B. Xu, D. Warde-Farley, S. Ozair, A. Courville and Y. Bengio, *Advances in neural information processing systems*, 2014.
 - 30 D. P. Kingma and M. Welling, *arXiv preprint arXiv:1312.6114*, 2013.
 - 31 G. L. Guimaraes, B. Sanchez-Lengeling, C. Outeiral, P. L. C. Farias and A. Aspuru-Guzik, *arXiv preprint arXiv:1705.10843*, 2017.
 - 32 B. Sanchez-Lengeling, C. Outeiral, G. L. Guimaraes and A. Aspuru-Guzik, 2017.
 - 33 T. Blaschke, M. Olivecrona, O. Engkvist, J. Bajorath and H. Chen, *Molecular informatics*, 2018, **37**, 1700123.
 - 34 R.-R. Griffiths and J. M. Hernández-Lobato, *Chemical science*, 2020, **11**, 577–586.
 - 35 T. Long, N. M. Fortunato, I. Opahle, Y. Zhang, I. Samathrakris, C. Shen, O. Gutfleisch and H. Zhang, *npj Computational Materials*, 2021, **7**, 66.
 - 36 M. Mokaya, F. Imrie, W. P. van Hoorn, A. Kalisz, A. R. Bradley and C. M. Deane, *Nature Machine Intelligence*, 2023, 1–9.
 - 37 M. Olivecrona, T. Blaschke, O. Engkvist and H. Chen, *Journal of cheminformatics*, 2017, **9**, 1–14.
 - 38 A. Furka, *Notarized Report (File number 36237/1982, in Hungarian)*, 1982.
 - 39 J. Degen, C. Wegscheid-Gerlach, A. Zaliani and M. Rarey, *ChemMedChem: Chemistry Enabling Drug Discovery*, 2008, **3**, 1503–1507.
 - 40 R. S. Bohacek, C. McMartin and W. C. Guida, *Medicinal research reviews*, 1996, **16**, 3–50.
 - 41 K. Klaus, *Principia Cybernetica Web*, 1986.
 - 42 C. E. Shannon, *ACM SIGMOBILE mobile computing and communications review*, 2001, **5**, 3–55.
 - 43 S. Kullback and R. A. Leibler, *The annals of mathematical statistics*, 1951, **22**, 79–86.
 - 44 *RDKit: Open-source cheminformatics*, <http://www.rdkit.org>, [Online; accessed 02-June-2022].
 - 45 S. A. Wildman and G. M. Crippen, *Journal of chemical information and computer sciences*, 1999, **39**, 868–873.
 - 46 P. Ertl, B. Rohde and P. Selzer, *Journal of medicinal chemistry*, 2000, **43**, 3714–3717.
 - 47 G. R. Bickerton, G. V. Paolini, J. Besnard, S. Muresan and A. L. Hopkins, *Nature chemistry*, 2012, **4**, 90–98.
 - 48 A. Alhossary, S. D. Handoko, Y. Mu and C.-K. Kwoh, *Bioinformatics*, 2015, **31**, 2214–2216.
 - 49 J. Schulman, F. Wolski, P. Dhariwal, A. Radford and O. Klimov, *arXiv preprint arXiv:1707.06347*, 2017.
 - 50 PubChem, *PubChem SARS-Cov-2 clinical trials*, <https://pubchem.ncbi.nlm.nih.gov/docs/covid-19>.
 - 51 H. Zhang, X. Gong, Y. Peng, K. M. Saravanan, H. Bian, J. Z. Zhang, Y. Wei, Y. Pan and Y. Yang, *Frontiers in chemistry*, 2022, **10**, 933102.
 - 52 Y. Wang, J. Xiao, T. O. Suzek, J. Zhang, J. Wang, Z. Zhou, L. Han, K. Karapetyan, S. Dracheva, B. A. Shoemaker *et al.*, *Nucleic acids research*, 2012, **40**, D400–D412.
 - 53 E. Hillhouse and D. Grammatopoulos, *Frontiers of hormone research*, 2001, **27**, 66–74.
 - 54 H. Kawasaki, G. M. Springett, N. Mochizuki, S. Toki, M. Nakaya, M. Matsuda, D. E. Housman and A. M. Graybiel, *Science*, 1998, **282**, 2275–2279.
 - 55 K.-H. Lin, G.-J. A. Wetzelaer, P. W. Blom and D. Andrienko, *Frontiers in Chemistry*, 2021, **9**, 800027.
 - 56 C. Bevington, A. J. Williams, C. Guider, N. C. Baker, B. Meyer, M. A. Babich, S. Robinson, A. Jones and K. A. Phillips, *Scientific Data*, 2022, **9**, 295.
 - 57 I. Morecroft, R. P. Heeley, H. M. Prentice, A. Kirk and M. R. MacLean, *British journal of pharmacology*, 1999, **128**, 730–734.
 - 58 K. M. Nautiyal, K. F. Tanaka, M. M. Barr, L. Tritschler, Y. Le Dantec, D. J. David, A. M. Gardier, C. Blanco, R. Hen and S. E. Ahmari, *Neuron*, 2015, **86**, 813–826.
 - 59 M. Clark and J. Neumaier, *Psychopharmacology bulletin*, 2001, **35**, 170–185.
 - 60 Y. Huang, W. A. Paxton, S. M. Wolinsky, A. U. Neumann, L. Zhang, T. He, S. Kang, D. Ceradini, Z. Jin, K. Yazdanbakhsh *et al.*, *Nature medicine*, 1996, **2**, 1240–1243.
 - 61 S. G. Sarafianos, B. Marchand, K. Das, D. M. Himmel, M. A. Parniak, S. H. Hughes and E. Arnold, *Journal of molecular biology*, 2009, **385**, 693–713.
 - 62 G. Ke, Q. Meng, T. Finley, T. Wang, W. Chen, W. Ma, Q. Ye and T.-Y. Liu, *Advances in neural information processing systems*, 2017.
 - 63 L. Espeholt, H. Soyer, R. Munos, K. Simonyan, V. Mnih, T. Ward, Y. Doron, V. Firoiu, T. Harley, I. Dunning *et al.*, *International conference on machine learning*, 2018, pp. 1407–1416.
 - 64 J. Schulman, F. Wolski, P. Dhariwal, A. Radford and O. Klimov, *arXiv preprint arXiv:1707.06347*, 2017.
 - 65 V. Mnih, A. P. Badia, M. Mirza, A. Graves, T. Lillicrap, T. Harley, D. Silver and K. Kavukcuoglu, *International conference on machine learning*, 2016, pp. 1928–1937.
 - 66 L. Kirsch, S. van Steenkiste and J. Schmidhuber, *arXiv preprint arXiv:1910.04098*, 2019.
 - 67 M. Riedmiller, R. Hafner, T. Lampe, M. Neunert, J. Degraeve, T. Wiele, V. Mnih, N. Heess and J. T. Springenberg, *International conference on machine learning*, 2018, pp. 4344–4353.